Effect of attack angle on flow characteristic of centrifugal fan

Effect of attack angle on flow characteristic of centrifugal fan

Y Wu[1], H S Dou[*1],Y K Wei[1], X P Chen[1], Y N Chen[2], W B Cao[2]

[1] Key Laboratory of Fluid Transmission Technology of Zhejiang Province, Zhejiang Sci-Tech University, Hangzhou, 310018, China
[2] Zhejiang Yilida Ventilator Co. Ltd., Taizhou, 318056, China

*E-mail: huashudou@yahoo.com

Abstract. In this paper, numerical simulation is performed for the performance and internal flow of a centrifugal fan with different operating conditions using steady three-dimensional incompressible Navier-Stokes equations coupled with the RNG k-e turbulent model. The performance curves, the contours of static pressure, total pressure, radial velocity, relative streamlines and turbulence intensity at different attack angles are obtained. The distributions of static pressure and velocity on suction surface and pressure surface in the same impeller channel are compared for various attack angles. The research shows that the efficiency of the centrifugal fan is the highest when the attack angle is 8 degree. The main reason is that the vortex flow in the impeller is reduced, and the jet-wake pattern is weakened at the impeller outlet. The pressure difference between pressure side and suction side is smooth and the amplitude of the total pressure fluctuation is low along the circumferential direction. These phenomena may cause the loss reduced for the attack angle of about 8 degree.

1. Introduction

Centrifugal fan is widely used in various industries of the national economy, and it is one of the main energy consuming equipment in the industrial and agricultural production. Thus, it is very important to enhance its performance [1]. According to statistics, the power consumption of various types of fans and pumps in China accounted for more than a third of the total power consumption. From the viewpoint of saving energy and reducing noise pollution, it is very important to design efficient centrifugal fans for saving energy [2]. Numerical simulation using computational fluid dynamics has gradually become an important method to understand the internal flow of fluid machinery. Only in the past few decades, the research of internal flow in the turbomachinery has evolved from the simplified model to the actual flow model, and from inviscid model to viscous model [3]. Liu et al [6] make statistical analysis of attack angle of the highest efficient point on the existing fifty kinds of centrifugal fans, reach a conclusion that the airflow attack angle of the highest efficient point in the actual fan is

negative ten degree to seventy degree. The airflow attack angle of the highest efficient point for the high efficient backward airfoil blade fan and backward plate blade fan is generally not more than positive six degree or negative six degree [7]. This is in good agreement with the design values recommended in the literatures [8-9]. Dou [10] simultaneously considered the effects of blade blocking and axial vortex, put forward the method of determining the geometrical angle of blades at impeller entrance. He gained that the efficiency of the centrifugal compressor is the highest when the airflow attack angle at the impeller entrance is six to eight degree, and gave an example for the calculation of attack angle. The optimal attack angle was about six degree obtained by the experiment of literature [10]. It has been proved that the optimal blade attack angle is about seven degree when considering the effect of the prewhirl angle by the experiment of literature [10]. The practical experience shows that the airflow attack angle at the highest efficient point of the fan is not necessarily zero degree due to the complexity of the actual air flow. Therefore, it is of great practical significance to design a highly efficient fan by the experiment and simulation.

In the paper, the flow characteristics of the fluid in the fan are studied using three-dimensional numerical simulation. The parameters of the whole flow field are obtained by using the finite volume method and SIMPLE algorithm to calculate Reynolds average Navier-Stokes equation. Then, the efficiency of a fan is calculated at various attack angles. And relevant analysis is carried out to clarify the origin of increasing efficiency at non-zero attack angle.

2. Governing equation

In this paper, the internal fluid flow characteristics of the 4-79-C type centrifugal fan used in Zhejiang Yilida Ventilator Incorporated Corporation are studied. For this type of fan, the specific speed is 67.4, the pressure coefficient is 0.91, and backward plate blade is adopted for the impeller vane. The governing equations are three-dimensional Reynolds average N-S equation and RNG $k-\varepsilon$ turbulence modle.

$$\begin{cases} \dfrac{\partial \overline{u_i}}{\partial x_i} = 0 \\ \rho u_j \dfrac{\partial \overline{u_i}}{\partial x_j} = \rho F_i - \dfrac{\partial \overline{p}}{\partial x_i} + \mu \dfrac{\partial^2 \overline{u_i}}{\partial x_j \partial x_j} - \rho \dfrac{\partial}{\partial x_j}(\overline{u_i u_j}) \end{cases} \tag{1}$$

The Realizable-$k-\varepsilon$ model is used for the turbulence model, which was proposed by Shih in 1995, which was considered as the coefficient C_μ of the calculation formula of the turbulent eddy viscosity coefficient μ_t was not constant [4-5], but it was related to the strain rate, in comparison with the standard $k-\varepsilon$ model, the ε equation had changed greatly, the production term in the k equation no longer contained the generated term P_k; the constraint equations of the turbulent kinetic energy k and the turbulent dissipation rate are as follows:

$$\frac{\partial(\rho k)}{\partial t} + \frac{\partial(\rho k u_j)}{\partial x_j} = \frac{\partial}{\partial x_j}\left[\left(\mu + \frac{\mu_t}{\sigma_k}\right)\frac{\partial k}{\partial x_j}\right] + \rho(P_k - \varepsilon) \tag{2}$$

$$\frac{\partial(\rho\varepsilon)}{\partial t}+\frac{\partial(\rho\varepsilon u_j)}{\partial x_j}=\frac{\partial}{\partial x_j}\left[\left(\mu+\frac{\mu_t}{\sigma_\varepsilon}\right)\frac{\partial\varepsilon}{\partial x_j}\right]+\rho C_1 E\varepsilon-\rho C_2\frac{\varepsilon^2}{k+\sqrt{\nu\varepsilon}} \tag{3}$$

where: $C_1=\max\left(0.43,\frac{\eta}{\eta+5}\right)$; $\eta=\left(2E_{ij}\cdot E_{ij}\right)^{1/2}\frac{k}{\varepsilon}$; $E_{ij}=\frac{1}{2}\left(\frac{\partial u_i}{\partial x_j}+\frac{\partial u_j}{\partial x_i}\right)$

constant values in the model: $\sigma_k=1.0$; $\sigma_k=1.2$; $C_2=1.9$.

3. Numerical method

In this paper, using Navier – Stokes equation and RNG k – ε turbulence model, the governing equation is discretized in space by finite volume method and two order upwind scheme. SIMPLE algorithm is used to solve the discrete equation, the convergence criterion is that the relative residual error of each variable is decreased by three orders of magnitude and the pressure difference is stable.

The inlet condition is velocity and outlet condition is outflow for the fan, the static and dynamic regions are set respectively by the multiple reference frame model(MRF), the wall condition is no slip boundary.

4. Verification of numerical method

4.1. Comparison of experiment and simulation

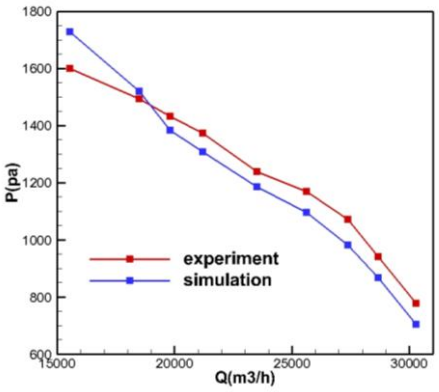

Fig 1. Curve of total pressure and flow rate.

The curve of total pressure and flow rate is shown in Figure 1. In this picture, the horizontal coordinate represents the flow rate, the vertical coordinate represents the total pressure. The red line is the experimental value, the blue line is the simulated value. As can be seen from Figure 1, the simulated value and experimental value of total pressure have same trend with flow rate. It is that the total pressure decreases with the increase of the flow rate, and they are in good agreement at different

conditions. Under the condition of small flow rate, the difference between the simulated value and experimental value is relatively large. The flow rate at design condition is small, and the difference between the simulated value and the experimental value is relatively small near design condition. The cause of above phenomenon may be that the non-steady composition is small under the condition of large flow rate and design flow rate, it has the little effect on the simulation of the flow field; under the condition of small flow rate, the non-steady composition is large, the effect and error are also large, but the error of simulation is within allowable error range, the result of simulation is correct.

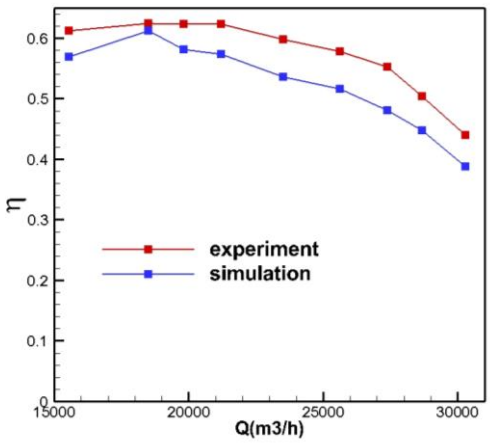

Fig 2. Curve of efficiency and flow rate.

The curve of efficiency and flow rate is shown in Figure 2. In the picture, the horizontal coordinate represents the flow rate, the vertical coordinate represents the efficiency. The red line is the experimental value, the blue line is the simulated value. As can be seen from Figure 2, the experimental efficiency and the simulated efficiency are in good agreement. The error is within allowable error range, the error may be caused by the simplified simulation model, the simulated efficiency is consistent with the experimental efficiency. Generally the numerical simulation method used in this paper is effective.

4.2. Verification of grid independence

The grid number is 2170000, 3620000 and 4900000, and the total pressure under design condition is calculated respectively, the result is shown in Figure 3.

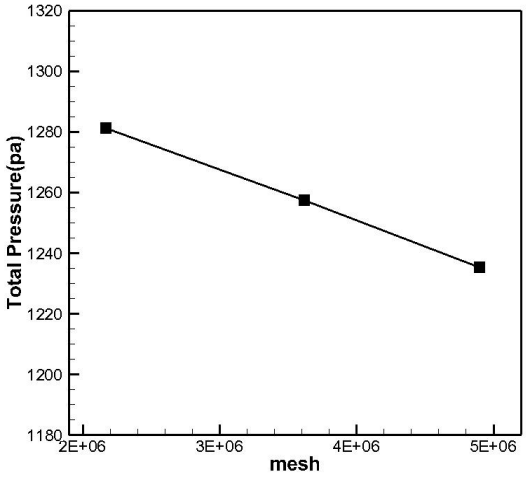

Fig 3. Total pressure under different mesh numbers.

The total pressure values under different grid numbers are shown in Figure 3, the relative errors between the simulated values and the experimental values are within three percent. It shows that the grid number has no effect on the calculation result, grid independence is proved.

5. Results and analysis of calculation

5.1. Example of calculation method

The geometrical parameters of the impeller are as follows: the impeller outlet diameter is $D_2 = 700mm$, the impeller inlet diameter is $D_1 = 488mm$, the impeller blade inlet width is $b_1 = 253.61mm$, the blade thickness is $S = 7mm$, the blade number is $Z = 16$. The rated rotation rate of impeller is $n = 1600r/m$, the blade inlet volume flow rate at design point is $V_1 = 6m3/s$. Assuming that there is no airflow prewhirl at the blade inlet, that is $C_{1u} = 0$, the calculation results are as follows:

The circumferential velocity at blade inlet:

$$\mathrm{U}_1 = \frac{\pi D_1 n}{60} = \frac{\pi \times 0.488 \times 1600}{60} = 40.88m/s$$

The airflow radial velocity at blade inlet:

$$C_{1r} = \frac{V_1}{\pi D_1 b_1} = \frac{6}{\pi \times 0.488 \times 0.25361} = 15.43m/s$$

The airflow angle at blade inlet:

$$tg\beta_1 = \frac{C_{1r}}{U_1} = \frac{15.43}{40.88} = 0.37745$$

$$\beta_1 = 20.68^\circ$$

The blocking factor at blade inlet:

$$\tau_1 = 1 - \frac{ZS}{\pi D_1 \sin\beta_{1A}} = 1 - \frac{16 \times 0.007}{\pi \times 0.488 \times \sin 25^\circ} = 0.827$$

Assuming that $\beta_{1A} = 25^\circ$ in the above formula, if the difference between the back calculation result and the assumption is large, the calculation needs to be repeated until they are consistent.

The airflow radial velocity at blade inlet only considering blade blocking:

$$C_{1r}{}' = \frac{C_{1r}}{\tau_1} = \frac{15.43}{0.827} = 18.66 m/s$$

The airflow angle at blade inlet only considering blade blocking:

$$tg\beta_1{}' = \frac{C_{1r}{}'}{U_1} = \frac{18.66}{40.88} = 0.45646$$

$$\beta_1{}' = 24.53^\circ$$

The airflow angle at blade inlet simultaneously considering the effect of blade blocking and axial vortex:

$$tg\beta_1{}'' = \frac{tg\beta_1}{\tau_1(1 - \frac{\pi}{Z}\sin\beta_{1A})} = \frac{0.37745}{0.827 \times (1 - \frac{\pi}{16} \times \sin 25^\circ)} = 0.4977$$

$$\beta_1{}'' = 26.46^\circ$$

$$\lambda = \beta_1{}'' - \beta_1 = 26.46^\circ - 20.68^\circ = 5.78^\circ$$

According to the reference [10], it is reasonable that the attack angle i is zero to two degrees smaller than λ. So we take $i = 4.78^\circ$

$$\beta_{1A} = \beta_1 + i = 20.68^\circ + 4.78^\circ = 25.46^\circ$$

The relative error between them is within two percent, which indicates that the hypothesis is reasonable.

5.2. Curve of efficiency and attack angle

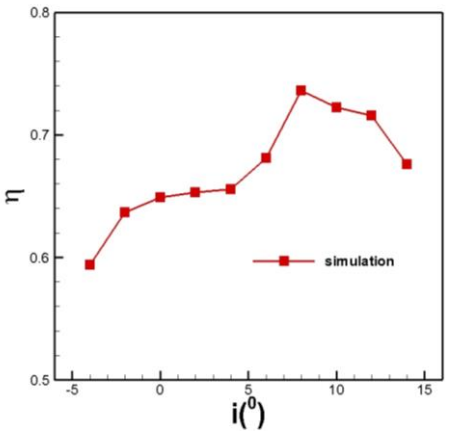

Fig 4. Broken line of efficiency and attack angle.

The broken line of efficiency and attack angle is shown in Figure 4. As can be seen from Figure 4, the efficiency is not the highest when the attack angle is zero degree under design condition. The efficiency is the highest when the attack angle is eight degree and not zero degree. The losses in the centrifugal fan are mainly composed of friction loss in the boundary layer of the impeller, loss caused by separation of boundary layer on the blades, loss from secondary flow, loss caused by the jet-wake pattern resulted from the nonuniform distribution of radial impeller outlet velocity [13]. In theory, the relative velocity angle β_1 of the airflow into the blades is in agreement with that the geometrical angle β_{1A} of blades when the attack angle is zero degree. The airflow enters the blade passage and doesn't impact into it, it makes the shock loss reduce to zero. But the practical experience shows that the airflow attack angle at the highest efficient point of the fan is not necessarily zero degree due to the complexity of the actual airflow. The larger the attack angle, the smaller the flow rate. In practical calculation, the efficiency of the fan is the highest when the flow rate is less than the design flow rate, which is consistent with the conclusions of relevant experiments in the literatures.

5.3. Total pressure distributions of different attack angles

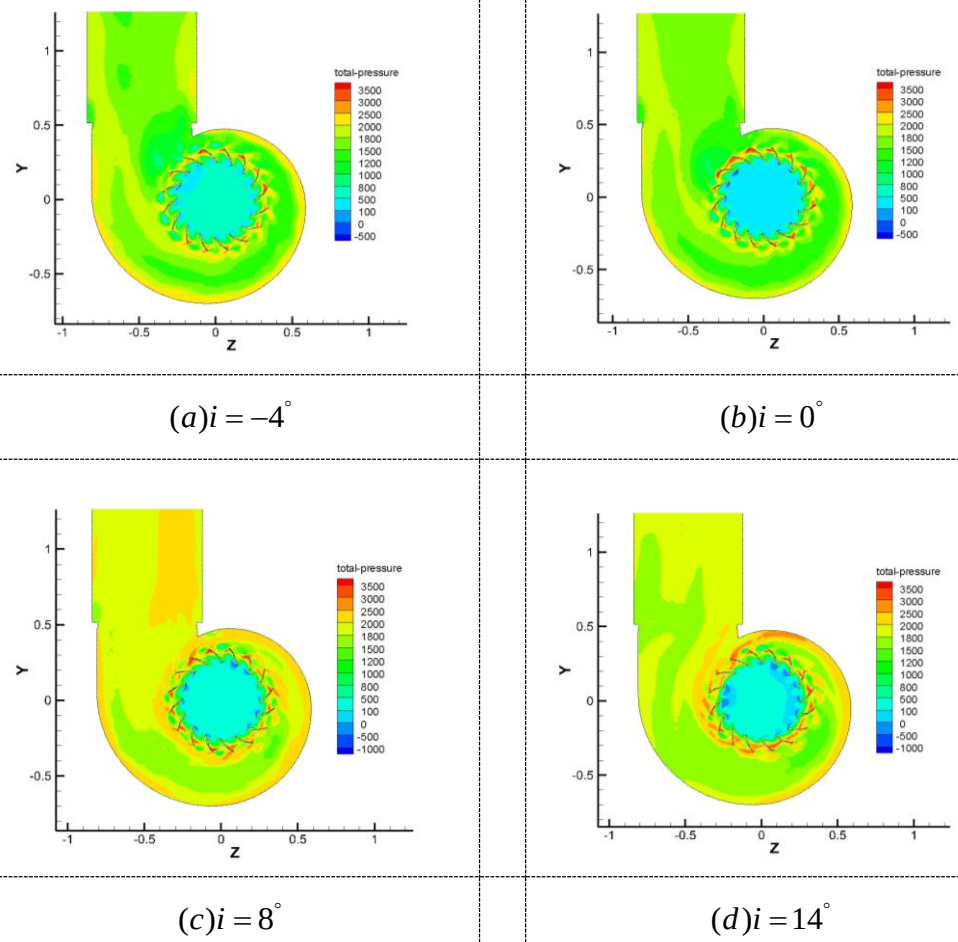

$(a) i = -4^{\circ}$ $(b) i = 0^{\circ}$

$(c) i = 8^{\circ}$ $(d) i = 14^{\circ}$

Fig 5. Total pressure charts of different attack angles.

The total pressure distribution at the same cross section is shown in Figure 5. As can be seen from Figure 5, the average total pressure of the fan cross section is the highest when the attack angle is eight degree, it indicates that the total energy is the largest. It takes the second place when the attack angle is fourteen degree, the average total pressure is lower when the attack angle is negative four degree and zero degree. Combined with the chart of efficiency and attack angle, the various energy losses of the airflow in the centrifugal fan are the least when the attack angle is eight degree, the various energy losses of the airflow are the largest when the attack angle is negative four degree. In the picture, it also can be seen that the total pressure is the lowest at the inner edge of the impeller in the centrifugal fan. And it increases gradually from the inside to the outside, the total pressure is the largest at the outer edge of the impeller. As far as the whole impeller channel is concerned, the total pressure is higher near the outlet side, the total pressure on the pressure side is the largest near the volute tongue, it is especially obvious when the attack angle is eight degree and fourteen degree. The total pressure in the volute wall is higher, and the total pressure changes of different attack angles in the volute are not uniform.

5.4. Static pressure distributions of different attack angles

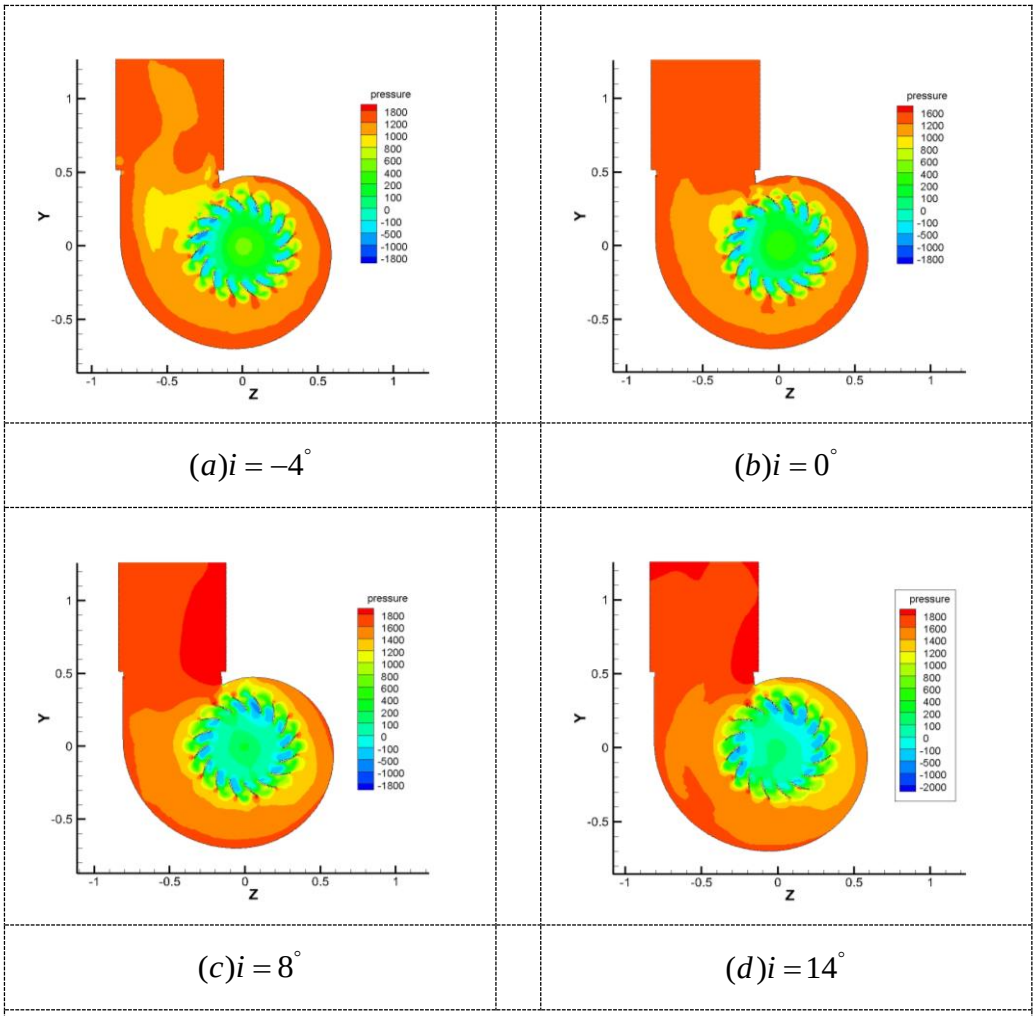

$(a)i=-4^{\circ}$ $(b)i=0^{\circ}$

$(c)i=8^{\circ}$ $(d)i=14^{\circ}$

Fig 6. Static pressure charts of different attack angles.

The static pressure distribution at the same cross section is shown in Figure 6. As can be seen from Figure 6, the static pressure is the largest in the extended section of the volute outlet, the volute wall and the volute tongue, the static pressure is the least near the impeller inlet. The static pressure is lower at the inner edge of the impeller, and it is higher at the outer edge of the impeller. The low pressure zone in the impeller channel is obvious when the attack angle is eight degree, and it extends from the impeller inlet to the middle part of the impeller channel. In the single impeller channel, the static pressure of the pressure surface is higher than that of the suction surface, which provides the condition for the formation of the secondary flow in the impeller channel. The hydrostatic pressure increases gradually from the center to the wall in the volute, the extended section of the volute outlet has an effect of diffusion, the hydrostatic pressure is the highest near the volute outlet.

5.5. Relative streamline charts of the impeller at different attack angles

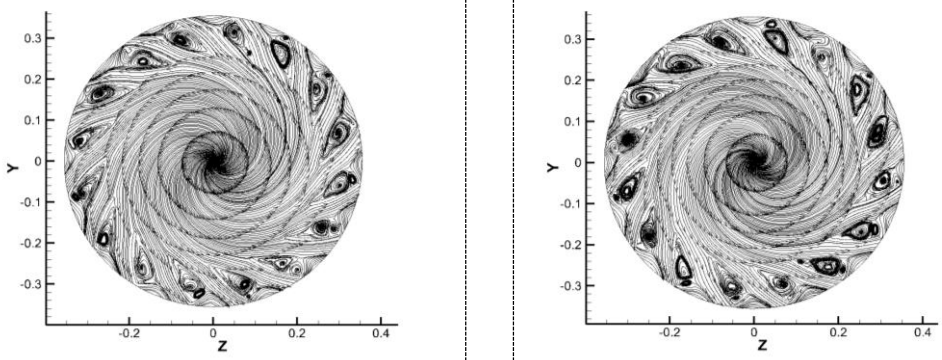

$(a) i = -4^{\circ}$ $(b) i = 0^{\circ}$

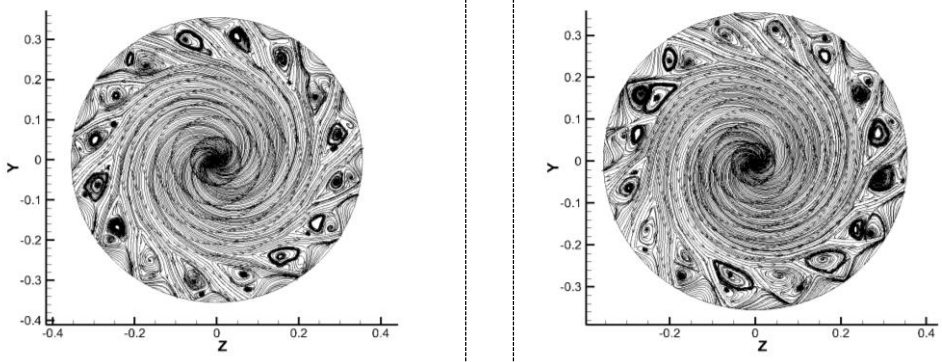

$(c) i = 8^{\circ}$ $(d) i = 14^{\circ}$

Fig 7. Relative streamline charts of different attack angles.

The relative streamline distribution at the same cross section is shown in Figure 7. From the figure 7, it can be seen that the flow in the impeller channel is not stable at different attack angles, and there is an obvious phenomenon of vortex and back flow. The flow in some impeller channels is not stable, which appears in the impeller channel outlet and the middle position of the impeller channel, the vortexes increase from the outlet to the inlet in some impeller channels, the flow is very unstable. Compared with the other three kinds of attack angles, when the attack angle is eight degree, the vortexes near the suction side are less in some impeller channels, the energy losses are smaller and the flow is smooth. At this time, the streamlines in the impeller channel are very uneven, the streamlines are not entirely along the curvature of the blade.

In fact, in the centrifugal impeller, the pressure of the blade pressure side is high, the velocity is low; the pressure of the blade suction side is low, the velocity is high, this pressure gradient causes the fluid micelle to be subjected to a force that points to the suction side. In the main flow region, the pressure gradient is balanced with the inertia force which is formed by the circular motion of the fluid micelle and the curvature of the blade. The velocity of the fluid micelle which is in the boundary layer of the blade and the wheel cap surface and the blade and the wheel plate surface is much smaller than

that in the main flow area. The inertia force formed can not be balanced with the above pressure gradient. Therefore, the flow is generated from the pressure surface to the suction surface in the boundary layer, the flow is perpendicular to the mainstream, it is the secondary flow [14]. The secondary flow makes the low velocity fluid micelles near the pressure surface sucked in the boundary layer of the wheel cap and that of the wheel plate, the low velocity fluid micelles are used to supplement the micelles with large kinetic energy, it makes the boundary layer of the suction surface thicker and leads to the separation of the boundary layer, this will form some vortex zones and cause some losses. The secondary flow causes the boundary layer thickness and separation of the suction surface, it inevitably affects the mainstream flow and reduces the relative velocity near the suction surface, the jet-wake is formed at the outlet of the impeller [15].

In the impeller channel, the relative streamlines of the fluid are close to the pressure surface. In the suction side, the fluid forms some vortexes, the fluid breaks away from the surface of the blade, which makes the flow separation at the end of the suction side and the wake loss. In some impeller channels, the vortexes severely block the flow channel when they are more intense in the impeller channel, the fluid flow along the radial outflow is seriously squeezed, the fluid produces relatively strong jet-wake at the impeller outlet, it causes the energy loss and affects the efficiency of the fan.

5.6. Turbulence intensity analysis of different attack angles

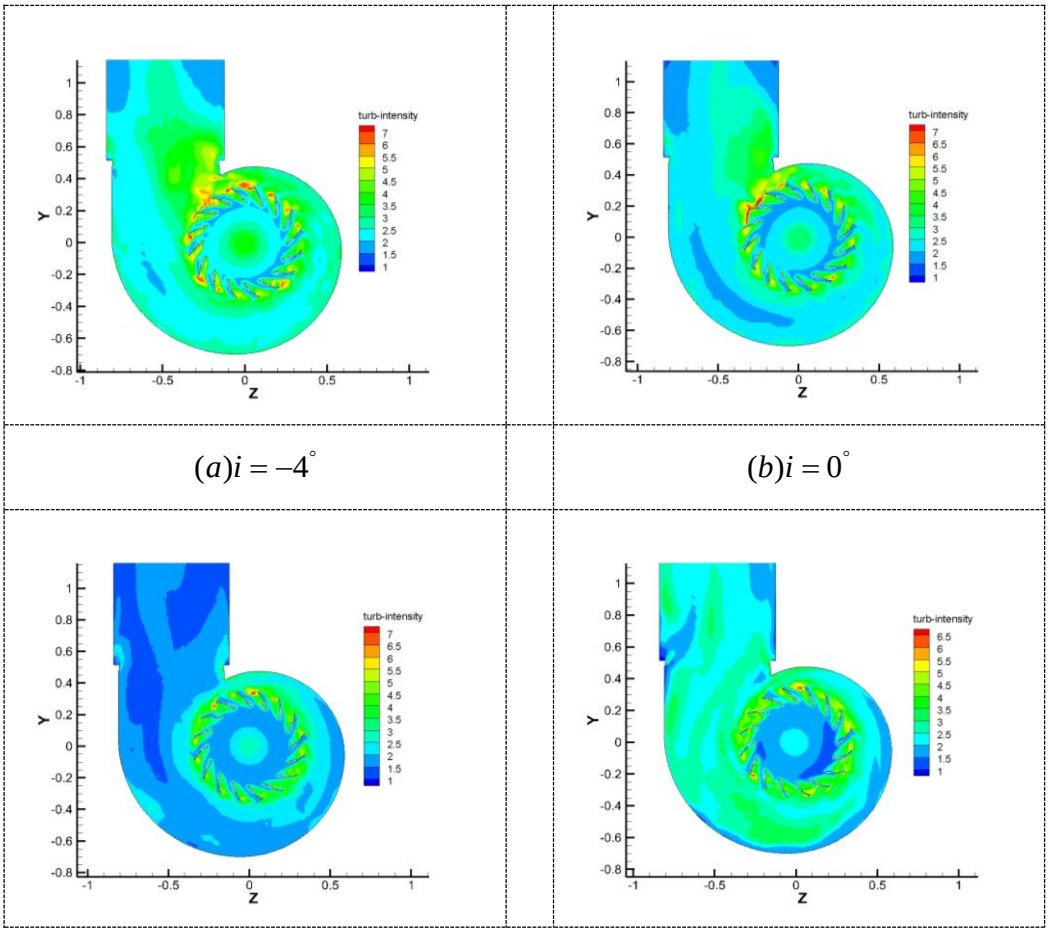

$(a) i = -4^{\circ}$ $(b) i = 0^{\circ}$

$(c)i=8^{\circ}$		$(d)i=14^{\circ}$

Fig 8. Turbulence intensity charts of different attack angles.

The turbulence intensity distribution at the same cross section is shown in Figure 8. The turbulence intensity is the degree that the wind velocity changes with time and space, which reflects the relative intensity of the fluctuating wind velocity, it is the most important feature of the atmospheric turbulence characteristics. The turbulence intensity is equal to the ratio of the mean square root of the turbulence fluctuating velocity and the average value of the turbulence fluctuating velocity [16]. As can be seen clearly from Figure 8, the turbulence intensity of the impeller is higher than that of the volute in the centrifugal fan, the turbulence intensity of the volute has a decreasing trend from the inside to the outside. In the impeller flow passage, the turbulence intensity of the suction surface is high, and the turbulence intensity of the pressure surface is low. The turbulence intensity of the volute is high, and the turbulence intensity at the outer edge of the suction surface of the impeller outlet is high near the volute tongue, it is particularly obvious when the attack angle is negative four and zero degree. When the attack angle is eight degree, the average turbulence intensity of the fan cross section is lower, and it is high at the other three angles.

5.7. Static pressure distribution of suction surface and pressure surface at different attack angles

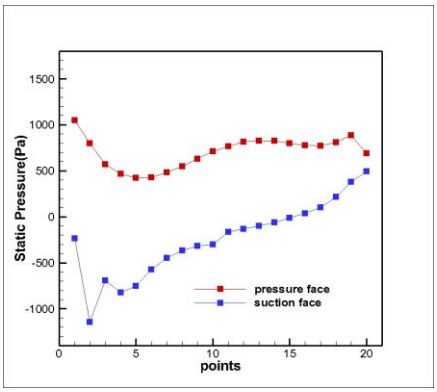

$(a)i=-4^{\circ}$

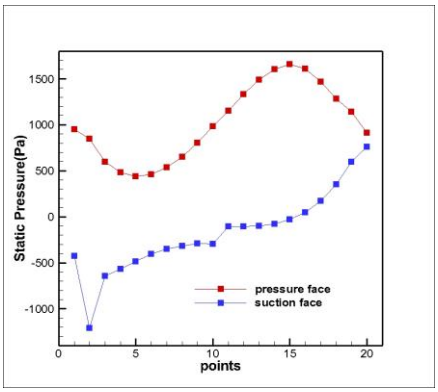

$(b)i=0^{\circ}$

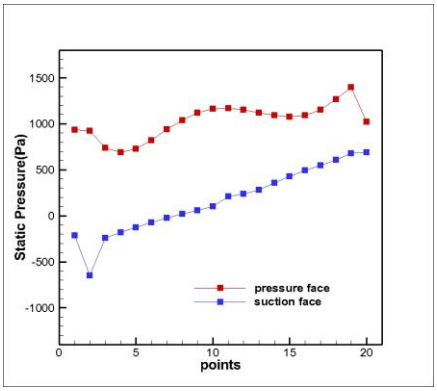

$(c)i = 8^{\circ}$

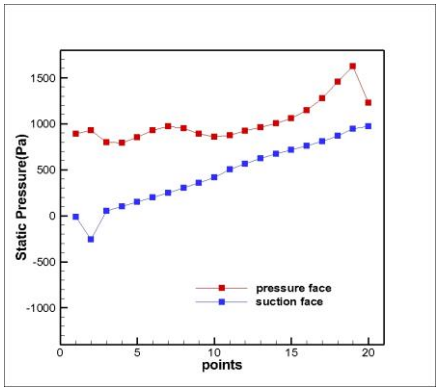

$(d)i = 14^{\circ}$

Fig 9. Static pressure charts of suction surface and pressure surface at different attack angles.

The pressure distribution on pressure and suction sides in a selected blade channel is shown in Figure 9. As can be seen from Figure 9, the horizontal coordinate represents the distance from the blade leading edge with interval on suction surface and pressure surface in the same impeller flow passage. The vertical coordinate indicates the static pressure, the red line is the static pressure of pressure surface, the blue line is the static pressure of suction surface. The distribution trend of the static pressure of the suction surface and the pressure surface in the impeller flow passage is generally consistent at different attack angles. The static pressure of the pressure surface is higher than that of the suction surface. Under the design condition, from the 15th point, the static pressure on the pressure side drops sharply, the static pressure on the suction side increases rapidly, this reduces the pressure difference between them. This causes the decrease of the work that the blades exert on the fluid. The comprehensive comparison of four pictures shows that the average static pressure difference between the pressure surface and suction surface is large and uniform. This causes the increase of the effective work that the blades exert on the fluid and the efficiency of the fan is also improved.

5.8. Pressure difference distribution between pressure side and suction side at different attack angles

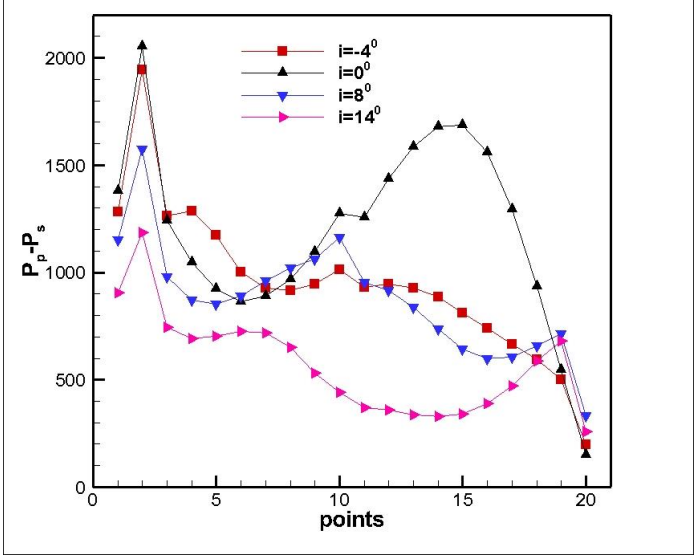

Fig 10. Pressure difference chart between pressure side and suction side at different attack angles.

The pressure difference in the selected blade channel is shown in Figure 10, which is adapted from Figure 9. As can be seen from Figure 10, the horizontal coordinate represents the distance from the blade leading edge with interval on suction surface and pressure surface in the same impeller flow passage. The vertical coordinate indicates the pressure difference between the pressure side and the suction side. In fact, the pressure surface is the working surface and the suction surface is the non-working surface in the impeller flow passage. The pressure is high and the velocity is low in the pressure side and the pressure is low and the velocity is high in suction side. The fluid is subjected to the force which direction is from the pressure side to the suction side, and the force exerts work on the fluid. It increases the velocity of the fluid. The pressure distribution at the pressure side and the suction side should be more uniform, and the pressure difference between them can not be too large. If the pressure difference is too large, the fluid will flow from the pressure side to the suction side. It will produce the back flow and vortex in the suction side, causing the energy loss and affecting the efficiency of the centrifugal fan, that we can see from Figure 11. When the attack angle is eight degree, the pressure difference between pressure side and suction side is smooth. While the attack angle is zero degree, the pressure difference in the second half is too large, which increases the load of the blades.

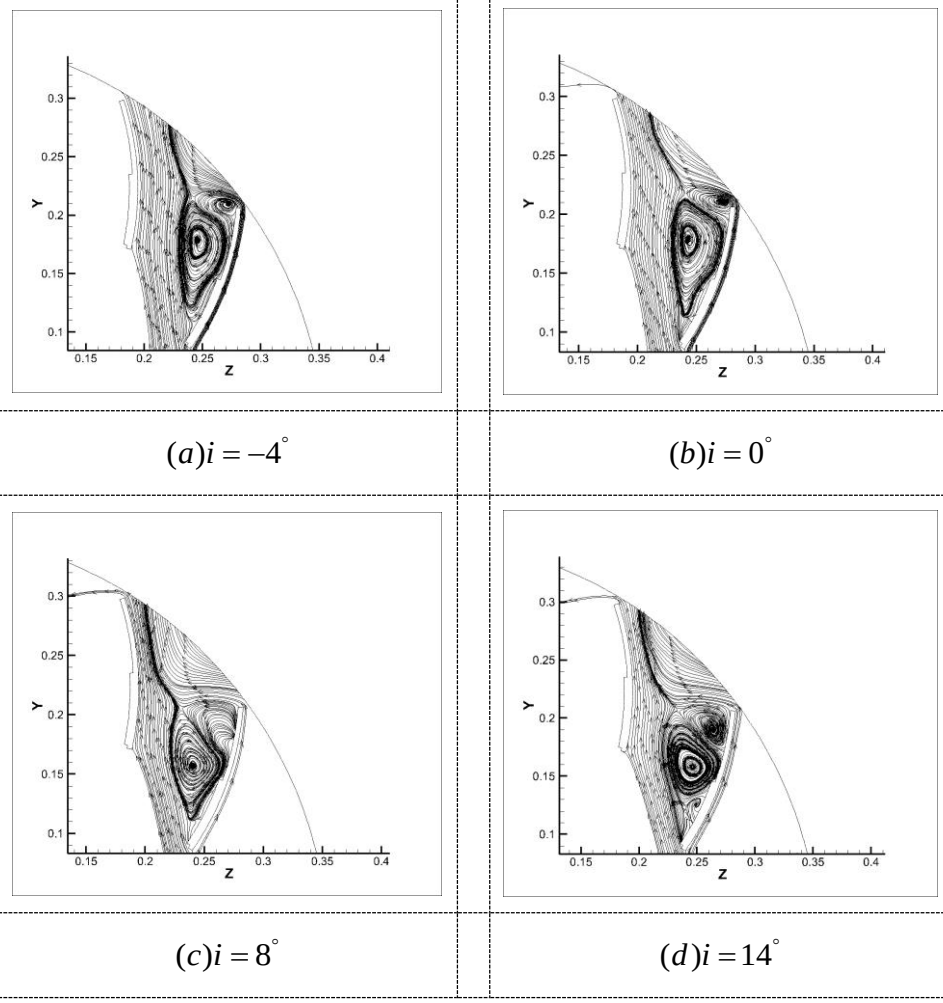

$(a) i = -4^{\circ}$ $(b) i = 0^{\circ}$

$(c) i = 8^{\circ}$ $(d) i = 14^{\circ}$

Fig 11. Relative streamlines charts of suction surface and pressure surface in the same impeller channel at different attack angles.

5.9. Velocity distribution of suction surface and pressure surface at different attack angles

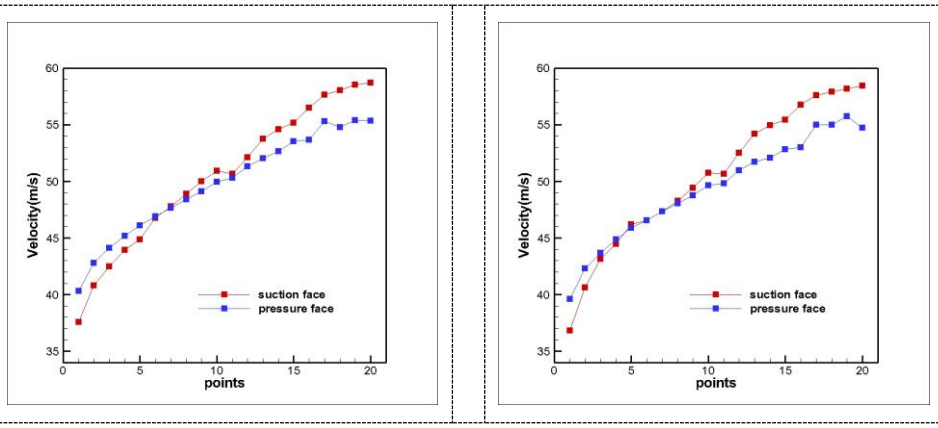

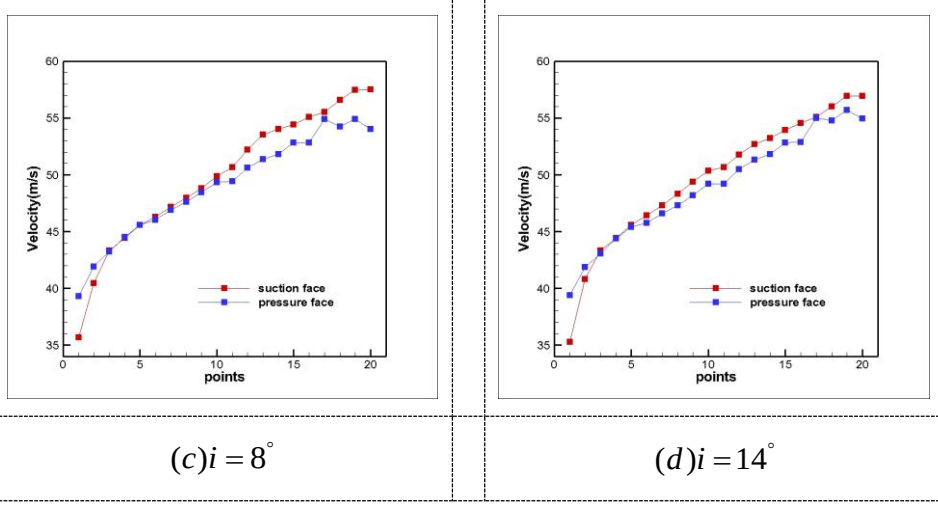

Fig 12. Velocity charts of suction surface and pressure surface at different attack angles.

The velocity distribution on pressure and suction sides in a selected blade channel is shown in Figure 12. As can be seen from Figure 12, the horizontal coordinate represents the distance from the blade leading edge with interval on suction surface and pressure surface in the same impeller flow passage. The vertical coordinate represents the velocity, the red line is the velocity of suction surface, the blue line is the velocity of pressure surface. The velocity distribution of suction surface and pressure surface in the same impeller flow passage is similar at different attack angles. The velocity of the pressure surface is higher than that of the suction surface near the inlet of the impeller, the velocity of the suction side is higher than that of the pressure side in the back section. When the fluid enters the impeller channel, the flow is relatively uniform, the velocity of the suction surface is close to that of the pressure surface. But the velocity of the pressure side is almost equal at the outlet of the impeller, the velocity of the suction side increases significantly at the inlet of the impeller. The velocity of the blade root is very small, it is because the flow is hindered when the fluid flows through the blade, it leads to a sudden drop in the velocity. While this position is close to the suction surface, so the velocity distribution of the starting part of the suction surface is affected. When the attack angle is eight degree, the average velocity difference between working face and non-working face for the blade is small. Which is particularly evident in the first section, it shows that the flow loss is smaller and the flow field distribution of the impeller outlet is more uniform. While the attack angle is zero degree, the velocity difference between suction side and pressure side in the second half is larger, the flow loss is larger and this will affect the efficiency of the fan.

5.10. Radial velocity distribution of the impeller channel outlet along the circumferential direction at different attack angles

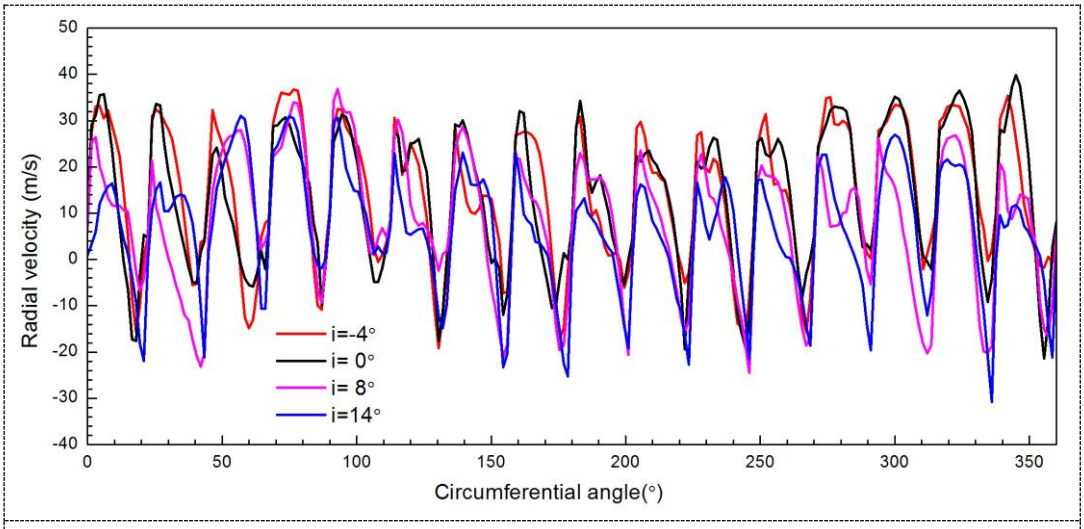

Fig 13. Chart of radial velocity and circumferential angle at different attack angles.

The radial velocity distribution of the impeller channel outlet along the circumferential direction is shown in Figure 13. As can be seen from Figure 13, when the attack angle is zero degree, the amplitude of the radial velocity fluctuation is large along the circumferential direction, this phenomenon can cause the jet-wake loss increased.

5.11. Static pressure distribution of the impeller channel outlet along the circumferential direction at different attack angles

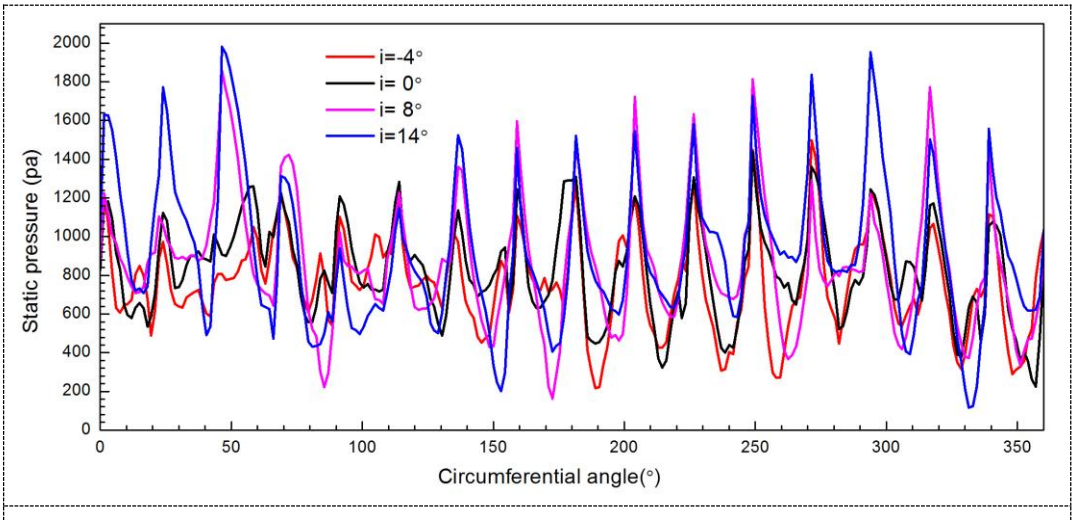

Fig 14. Chart of static pressure and circumferential angle at different attack angles.

The static pressure distribution of the impeller channel outlet along the circumferential direction is shown in Figure 14. As can be seen from Figure 14, when the attack angle is fourteen degree, the amplitude of the static pressure fluctuation is large along the circumferential direction, it may cause the instability in the flow and the loss increased.

5.12. Total pressure distribution of the impeller channel outlet along the cirumferential direction at different attack angles

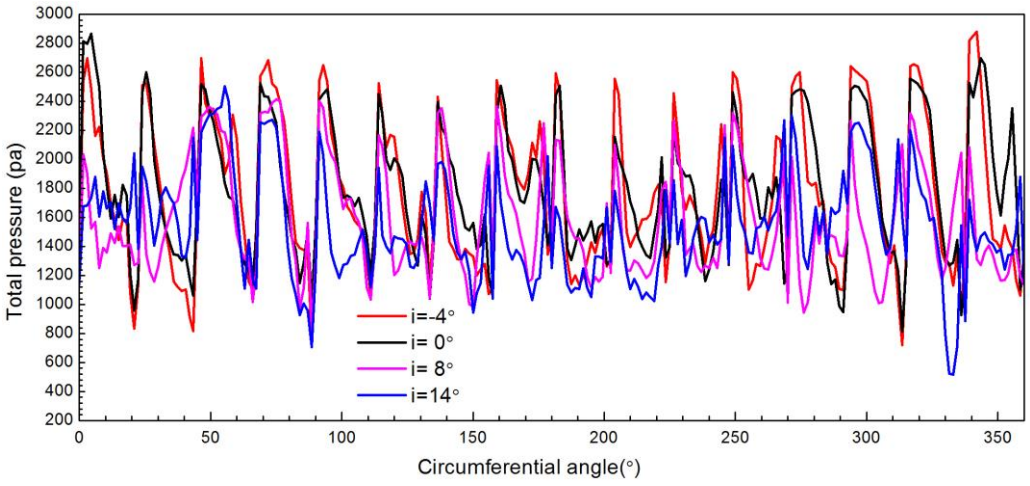

Fig 15. Chart of total pressure and circumferential angle at different attack angles.

The total pressure distribution of the impeller channel outlet along the circumferential direction is shown in Figure 15. As can be seen from Figure 15, when the attack angle is eight degree, the amplitude of the total pressure fluctuation is low along the circumferential direction. This phenomenon may cause the loss reduced.

5.13. Velocity distribution of the impeller channel outlet along the circumferential direction at different attack angles

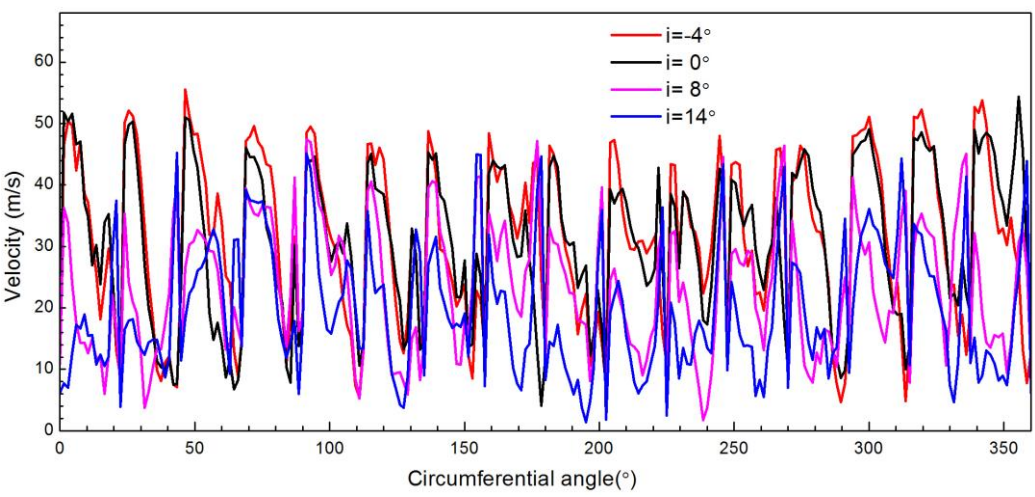

Fig 16. Chart of velocity and circumferential angle at different attack angles.

The velocity distribution of the impeller channel outlet along the circumferential direction is shown in Figure 16. As can be seen from Figure 16, when the attack angle is eight degree, the amplitude of the

velocity fluctuation is low along the circumferential direction, which indicates the velocity is stable and the loss is less.

5. Conclusions

(1) In this paper, the efficiency of the centrifugal fan is calculated at various attack angles. The efficiency is the highest when the attack angle is about eight degree. The numerical simulation of the fan model shows that the maximum efficiency point of the centrifugal fan is not at the zero attack angle condition, while the efficiency is the highest when the attack angle is eight degree.

(2) The average total pressure is the highest when the attack angle is six to eight degree, which indicates that the total energy is highest, it has a direct impact on the efficiency of the fan.

(3) When the attack angle changes, the flow has obvious vortex and reflux in the impeller channel. The reflux occurs in the outlet and intermediate position in some impeller channels, the vortex gradually increases from the outlet to the inlet in partial impeller channels. Some separated vortexes form near the suction side of the impeller channel. The jet-wake forms in the outlet of the impeller channel. The vortex loss, the separation loss of boundary layer and the jet-wake loss in the impeller will affect the efficiency of the centrifugal fan.

(4) When the attack angle is in the range of six to eight degree, the flow is smooth and uniform in some impeller channels, the vortexes are reduced and weaker in the suction side.

(5) When the attack angle is eight degree, the pressure difference between pressure side and suction side is smooth. While the attack angle is zero degree, the pressure difference in the second half is too large, which increases the load of the blades. If the pressure difference is too large, the fluid will flow from the pressure side to the suction side, it will produce the back flow and vortex in the suction side, cause the energy loss and affect the efficiency of the centrifugal fan.

(6) When the attack angle is eight degree, the amplitude of the total pressure fluctuation is low along the circumferential direction. This phenomenon may cause the loss reduced.

Acknowledgments

This work is supported by Zhejiang Province Key Science and Technology Innovation Team Project (2013TD18) and the National Natural Science Foundation of China (51579224).

References

[1] Li X H, He H W, Gong W Q and Huang S J, 2002, Numerical simulation of steady flow for the whole machine in centrifugal fan, *Journal of engineering thermal physics*, **23**(4):453-456 (in Chinese).

[2] Zhao L F, 2005, Flow field simulation optimization design of centrifugal fan, *PhD Thesis of Dalian Jiaotong University* (in Chinese).

[3] Peng F, 2004, Three dimensional numerical calculation and research of centrifugal fan, *PhD Thesis of Wuhan University of Technology* (in Chinese).

[4] Shih T H, Liou W W, Shabbir A, Yang Z and Zhu J, 1995, A new k-ε Eddy-viscosity model for high Reynolds number turbulent flows, *Computer & Fluids*, **24**(3): 227-238.

[5] Bhope D V, Padole P M, Bhope D V and Padole P M, 2004, Experimental and theoretical analysis of stresses, noise and flow in centrifugal fan impeller, *Mechanism & Machine*

Theory, **39**(12): 1257-1271.

[6] Liu G Z, Wang X J and Gao Y, 2004, Function curve of the optimum attack angle of centrifugal fan, *Fan technology*, (3): 1-3 (in Chinese).

[7] Pan D L, 2009, Discussion on the optimum attack angle of centrifugal fan, *Fan technology*, (1): 13-15 (in Chinese).

[8] Li Q Y, 1981, Fan, *Mechanical industry press*, 20-25 (in Chinese).

[9] Shenyang Institute of blower and Northeast Engineering Institute, 1984, Centrifugal fan, *Mechanical industry press*, 7-11 (in Chinese).

[10] Dou H S, 1986, The method of determining the geometrical angle of blades at impeller entrance of centrifugal compressors, *Fan technology*, (4): 6-10 (in Chinese).

[11] Gu F, Engeda A, Cave M and Liberti J L D, 2001, A Numerical Investigation on the Volute/Diffuser Interaction Due to the Axial Distortion at the Impeller Exit, *Journal of Fluids Engineering*, **123**(3):475-483.

[12] Jeon W H and Lee D J, 2003, A numerical study on the flow and sound fields of centrifugal impeller located near a wedge,*Journal of Sound & Vibration*, **266**(4):785-804.

[13] Wu C, Zhao J, Sai Q Y, Li M, Zhou D S and Hu S G, 2001, Study on the influence of impeller structure on the flow characteristic and performance of centrifugal fan, *Mechanical research and application*, (6): 34-36 (in Chinese).

[14] Cheng X D, 2006, Centrifugal fan, *Beijing: Chemical Industry Press*, 4-8 (in Chinese).

[15] Wu Y L, Chen Q G and Liu S H, 2011, Fan and compressor, *Tsinghua University press*, 20-24 (in Chinese).

[16] Yu J M, Li S and Hao J Z, 2011, Numerical analysis of the flow characteristic of centrifugal fan, *Fluid machinery*, **39**(9): 34-37 (in Chinese).